Biophysical Journal
Article

Biophysical Society

Different membrane order measurement techniques are not mutually consistent

Ankur Gupta,[1] Mamata Kallianpur,[1] Debsankar Saha Roy,[1] Oskar Engberg,[2] Hirak Chakrabarty,[3] Daniel Huster,[1,2,*] and Sudipta Maiti[1,*]

[1]Tata Institute of Fundamental Research, Colaba, Mumbai, India; [2]Institute of Medical Physics and Biophysics, University of Leipzig, Leipzig, Germany; and [3]School of Chemistry, Sambalpur University, Burla, Odisha, India

ABSTRACT "Membrane order" is a term commonly used to describe the elastic and mechanical properties of the lipid bilayer, though its exact meaning is somewhat context- and method dependent. These mechanical properties of the membrane control many cellular functions and are measured using various biophysical techniques. Here, we ask if the results obtained from various techniques are mutually consistent. Such consistency cannot be assumed a priori because these techniques probe different spatial locations and different spatial and temporal scales. We evaluate the change of membrane order induced by serotonin using nine different techniques in lipid bilayers of three different compositions. Serotonin is an important neurotransmitter present at 100s of mM concentrations in neurotransmitter vesicles, and therefore its interaction with the lipid bilayer is biologically relevant. Our measurement tools include fluorescence of lipophilic dyes (Nile Red, Laurdan, TMA-DPH, DPH), whose properties are a function of membrane order; atomic force spectroscopy, which provides a measure of the force required to indent the lipid bilayer; ^{2}H solid-state NMR spectroscopy, which measures the molecular order of the lipid acyl chain segments; fluorescence correlation spectroscopy, which provides a measure of the diffusivity of the probe in the membrane; and Raman spectroscopy, where spectral intensity ratios are affected by acyl chain order. We find that different measures often do not correlate with each other and sometimes even yield conflicting results. We conclude that no probe provides a general measure of membrane order and that any inference based on the change of membrane order measured by a particular probe may be unreliable.

SIGNIFICANCE This work highlights the need for understanding the response of different techniques used in investigating lipid membrane order. Inference about the increase (or decrease) of membrane order measured by any particular technique is typically assumed to be valid irrespective of the biophysical tool used. However, these techniques measure somewhat different properties related to membrane order, and there is no a priori reason for them to be in agreement. Our systematic study involving nine different methods shows that the outputs of these measurements do not universally correlate with each other. Moreover, they frequently show opposite directions for the change of membrane order under a specific perturbation that is biologically relevant. Thus, interpretation of biological consequences by measuring the membrane order using a single probe may be unreliable.

INTRODUCTION

The term "membrane order" is generally used to describe the mechanical properties of lipid bilayer membranes. Mechanical properties play a crucial role in various key cellular functions such as structure and functions of membrane proteins (1), signal transduction (2–5), receptor translocation (6), and mitochondria metabolism (7). Studies showed that alteration in membrane order causes cellular dysfunction (8–11) and acts as a reporter for identifying and targeting many diseases (12–14). Though membrane order typically relates to lipid packing and dynamics in the membrane, its definition is context dependent. A large range of biophysical techniques has been developed to measure this quantity. Any inference drawn from a measurement performed with a particular technique will be robust only when it is known that it correlates well with other techniques. In this work, we have measured membrane order using multiple techniques to evaluate the correlation among these measurements.

Environment- and polarity-sensitive fluorescent dyes are the most commonly used probes of membrane order because

Submitted June 7, 2022, and accepted for publication August 19, 2022.

*Correspondence: daniel.huster@medizin.uni-leipzig.de or maiti@tifr.res.in

Editor: Michael F. Brown.

https://doi.org/10.1016/j.bpj.2022.08.029

of their compatibility with live-cell measurements (15–18). For example, the maximum emission peak in the fluorescence spectrum of the dye Nile Red shifts to a lower wavelength if the environment becomes less polar. The lower polarity inside the membrane is a result of the tighter packing of hydrophobic lipid tails, which indicates an increase in membrane order (19). Therefore, a ratio of the Nile Red emission in the green region (569–604 nm) to that in the red region (624–659 nm), the so-called G/R ratio, provides a measure of membrane order. The other commonly used membrane polarity-sensitive dye is Laurdan (20), which has a red-shifted fluorescence emission (peak at ~490 nm) in disordered membranes and a blue-shifted fluorescence in ordered membranes (peak at ~440 nm). The order of the membrane is quantified by a ratiometric parameter, known as generalized polarization (GP). GP is defined as a normalized ratio of fluorescence intensities $(I_{440} - I_{490})/(I_{440} + I_{490})$ (20). It has been shown that the GP of Laurdan is linearly dependent on membrane tension in model membranes (21). Other fluorescent probes such as Prodan, DPH, TMA-DPH, pyrene and its derivatives, N-(7-Nitrobenz-2-oxa-1,3-diazol-4-yl), and DiI are also used to determine membrane order (22). Eight different polarity-sensitive dyes have been shown (23) to have a reasonably good qualitative correlation for membrane order measurement, though they have different sensitivities, likely due to their local position and orientation (22). However, Laurdan and Patman fluorescence spectra (24) do not seem to correlate in their sensitivity to membrane cholesterol molar fraction.

There are other techniques to probe the order of the membrane, such as atomic force microscopy (AFM), fluorescence correlation spectroscopy (FCS), Raman spectroscopy, and NMR. AFM measures the stiffness of the membrane by measuring the amount of force (known as breakthrough force) required to rupture the bilayer locally by a sharp AFM tip (25,26). In general, higher stiffness (i.e., greater breakthrough force) is correlated with higher ordering of the membrane. FCS measures the translational diffusion coefficients (D_T) of membrane lipids (27). A smaller D_T indicates a more ordered membrane. Z-scan FCS is a special FCS methodology employed to determine the diffusion coefficient of planar-supported bilayers and avoids nontrivial external calibration of the size of the detection volume (28). Raman spectroscopy is also used to measure the order of the membrane. The Raman spectra of the ν(C-H) region of the membrane are sensitive to lipid packing and local lipid dynamics (29,30). Specifically, the ratios of intensities I_{2885}/I_{2850} and I_{2850}/I_{2930} provide the average CH_2 conformational order (or lateral order) and terminal CH_3 rotational order of the membrane. These ratios are related to the order of the membrane. Perhaps the most direct atomic-level measurement of the order of the lipid acyl chains can be obtained from solid-state NMR measurements. Time-averaged orientational fluctuations of the C–^{2}H bond vectors of lipid chains, obtained from residual quadrupolar couplings measurement in ^{2}H NMR, give the orientational (or segmental) order parameter for each C–^{2}H group (31–33). The same information is also available from measurements of the motionally averaged ^{1}H-^{13}C dipolar couplings under magic angle spinning conditions (34,35).

Typically, inferences on membrane order are drawn from studies using a single membrane probe (36–40). A few studies have utilized multiple types of membrane probes to determine the order of the membrane and observed good qualitative correlation between GP and bending rigidity measurements (41), NMR order parameter and GP measurements (42), and GP and AFM breakthrough force (F_X) measurements (26). However, these studies have used only a few probes (two or three) and a single membrane composition. Thus, it is not obvious whether the correlation is universal among a large range of techniques and different types of bilayers.

Here, we have expanded the number of techniques to nine, applying them to lipid bilayers consisting of POPC (1-palmitoyl-2-oleoyl-glycero-3-phosphocholine)/POPG (1-palmitoyl-2-oleoyl-sn-glycero-3-phospho-(1'-rac-glycerol))/cholesterol in the molar ratio of 1/1/1 (PPC111). A subset of these techniques was also applied to several different membrane compositions. The techniques we employed were AFM, NMR, z-scan FCS, Raman, and fluorescence spectroscopy of Nile Red, Laurdan, DPH, and TMA-DPH dyes. Instead of correlating absolute values of the membrane order, we have assessed the change in membrane order induced by a perturbation, arguing that a change in membrane order should correlate more strongly across different probes and techniques. The perturbative agent is serotonin, a neurotransmitter whose interaction with the lipid membrane has been a focus of recent biophysical research (25,43–47). We used the small lipophilic molecule serotonin to induce changes in membrane order. Serotonin and serotonin-like molecules modulate membrane order, as shown by our previous studies (25,46–48). We compared both the magnitude and the direction of change for each of these systems and found that the values and the directions frequently do not correlate between techniques.

MATERIALS AND METHODS

The details of the materials and methods are provided in the supporting material. In brief, supported bilayers (SLBs) are prepared on the freshly cleaved mica substrates by following the vesicle fusion method (49). The different compositions were pure POPG, POPC/POPG/cholesterol at a molar ratio of 1/1/1 (PPC111), and DOPC (1,2-dioleoyl-sn-glycero-3-phosphocholine)/egg sphingomyelin/cholesterol at a molar ratio of 2/2/1/ (DEC221). The AFM force indentation study was performed on the SLBs using a commercial NanoWizard II system. The membrane was ruptured locally by the AFM tip, and the force required to rupture it is quantified as F_X. The fluorescence spectra of Nile Red incubated SLBs were obtained by performing confocal imaging in the lambda stacking mode on the commercial LSM 880. One μM Nile Red was incubated to SLBs for 20 min, and unbound Nile Red was washed thoroughly. The multiphoton imaging of Laurdan incubated SLBs is performed by exciting the Laurdan using a

780 nm pulsed laser source and collecting the emission in two channels—blue (410–440 nm) and green (485–515). These channel images were used to obtain GP of Laurdan in the membrane. The diffusion coefficients of lipids in the SLBs were obtained by performing z-scan FCS. The autocorrelation curves were obtained at different z-intervals (along the bilayer axis) using a home-built AFM-confocal instrument and fitted to obtain diffusion coefficients of lipids in the SLBs. The Raman spectra and corresponding ratios I_{2885}/I_{2850} and I_{2850}/I_{2930} were obtained by recording the Raman spectra of SLBs with a home-built line-confocal Raman microscope. Steady-state anisotropy of DPH and TMA-DPH was measured using Hitachi F-7000 (Japan) spectrofluorometer. Both the fluorophores were excited at 360 nm, and the corresponding emissions were measured at 430 nm. For ^{2}H solid-state NMR, multilamellar vesicles were produced by codissolving lipids and serotonin in organic solvents; after evaporating the solvents and lyophilization, the samples were hydrated and equilibrated by freeze thawing. Order parameter profiles were calculated from the dePaked ^{2}H NMR spectra of the deuterated lipid measured on a Bruker 750 Avance I NMR spectrometer (33).

RESULTS

Serotonin-induced perturbation of PPC111 membranes

AFM force indentation

In our previous studies (25), we have measured the F_X of PPC111 SLBs in the absence and the presence of 5 mM serotonin using the AFM force indentation technique. Fig. 1 *B* (reproduced from Dey et al. (25)) shows the representative histograms of F_X of PPC111 in the absence (black) and the presence (red) of 5 mM serotonin. The histogram shows that the F_X of the PPC111 bilayer decreases by 58% ± 19% (25), suggesting that the PPC111 bilayer becomes more disordered in the presence of 5 mM serotonin.

Spectral imaging of Nile Red

We have performed the spectral imaging of the lipophilic dye Nile Red bound to PPC111 SLB in the absence and the presence of 5 mM serotonin to measure the serotonin-induced change in the Nile Red fluorescence spectra. The serotonin-containing membrane has clearly blue-shifted fluorescence spectra (Fig. 1 *D*, *red*) compared with that without serotonin (Fig. 1 *D*, *black*). We have calculated the G/R ratio to quantify the membrane order by Nile Red. The average G/R ratio in the absence and presence of serotonin is 0.73 ± 0.07 and 1.13 ± 0.03, respectively. Thus, the average G/R increases by 55% ± 12%. This suggests that the PPC111 membrane becomes more ordered after 5 mM serotonin addition.

Spectral imaging of Laurdan

We have performed multiphoton imaging (which effectively accesses the UV excitation wavelengths using near infrared light) of the lipophilic Laurdan dye bound to PPC111 SLB in the absence and the presence of 5 mM serotonin to measure the channel-specific fluorescence intensity and then processed them to obtain GP images. Serotonin was incubated with the bilayer for 45 min. The multiphoton imaging was required, as conventional fluorimeter measurements cannot be performed on the SLBs. The representative GP images of the PPC111 SLB in the absence and presence of 5 mM serotonin are shown in Fig. 1 *H* and *L*, respectively. The average GP value of the PPC111 bilayer in the absence (Fig. 1 *M*, *black bar*) and in the presence (Fig. 1 *M*, *red bar*) of 5 mM serotonin are 0.48 ± 0.02 and 0.63 ± 0.01, respectively. The average GP value increases by 31% ± 5% in the presence of 5 mM serotonin, indicating that the PPC111 bilayer becomes more ordered in the presence of serotonin.

Steady-state anisotropy of DPH and TMA-DPH dyes

We have performed the steady-state anisotropy measurement of PPC111 vesicles doped with DPH and TMA-DPH dyes with increasing concentrations of serotonin to measure the rotational dynamics of probes in the vesicles, which in turn provides the information of lipid packing or membrane order. DPH is located at an average distance of approximately 7.8 Å from the center of the bilayer, whereas its trimethylammonium derivative (TMA-DPH) partitions at the interfacial region of the membrane (10.9 Å from the center of the bilayer) because of its charge. Therefore, fluorescence anisotropy of DPH and TMA-DPH provide information of membrane order at two different regions of the membrane (50). We found that rotational anisotropy increases in the presence of serotonin in both dyes (Fig. 1 *N* and *O*). The average anisotropy of DPH and TMA-DPH increases by 38% ± 3% and 5% ± 1% at 0.5 mM serotonin, respectively. This suggests that the rotation of lipids slowed down in the presence of serotonin in the PPC111 vesicles, indicating that the membrane becomes more ordered in the presence of serotonin.

Raman spectroscopy measurements

The Raman spectra of PPC111 SLB in the absence and presence of 20 mM serotonin are measured at ∼ 2850, ∼2885, and ∼2930 cm^{-1}. The representative normalized Raman spectra for fresh PPC111 SLB (black) and serotonin-containing SLB (light brown) are shown in Fig. 1 *P*. For the PPC111 membrane, serotonin showed an average increase of 11% ± 2% in the I_{2885}/I_{2850} ratio, indicating an increase of the CH_2 conformational order (Fig. 1 *Q*, *left*). However, the I_{2850}/I_{2930} ratio decreases by 45% ± 3% (Fig. 1 *Q*, *right*), suggesting that the local order near the terminal CH_3 decreases upon incubation with serotonin.

Solid-state NMR

In a previous study (25), we had also measured the ^{2}H NMR order parameter of the PPC111 vesicles in the absence and the presence of 10 mol % serotonin (relative to the lipid) using ^{2}H solid-state NMR. The NMR measurements have shown that the order parameter of the PPC111 bilayer along the lipid acyl chains for deuterated POPC and POPG decreases in the presence of serotonin both at 25°C and 37°C (Fig. 1 *R*, reproduced from Dey et al. (25)). This

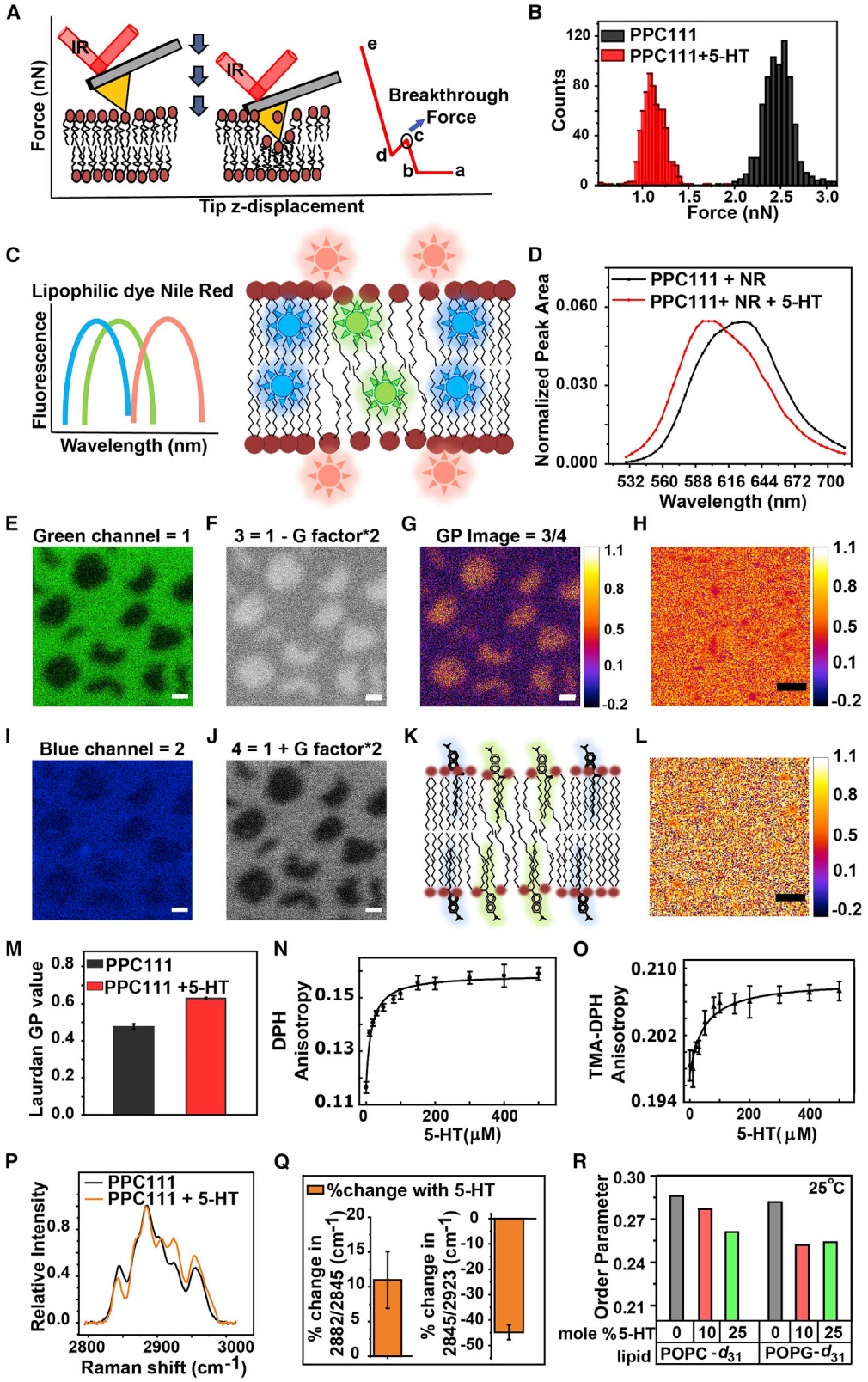

FIGURE 1 Effect of serotonin on the mechanical properties of PPC111 bilayer probed by different biophysical techniques. (*A*) Schematic of the AFM force indentation studies. (*B*) A representative histogram of breakthrough forces on the PPC111 bilayer in the absence (*black*) and presence (*red*) of 5 mM serotonin (reproduced from Dey et al. (25)). (*C*) Schematic of the fluorescence spectral properties of Nile Red in different membrane environments. (*D*) Fluorescence spectra of membrane-bound Nile Red dye in PPC111 bilayer in the absence (*black*) and presence (*red*) of 5 mM serotonin (average of $N = 3$

(legend continued on next page)

suggests that the PPC111 membrane becomes more disordered upon adding serotonin.

Serotonin induced perturbations of POPG and DEC221 membranes

The investigations of the PPC111 membrane suggested that different techniques and probes used to measure the membrane order frequently do not provide results that correlate with each other. To investigate if this is peculiar to the type of membrane we have used, we probed two other membrane compositions, POPG and DEC221. Among these, DEC221 is a biphasic bilayer, and the ordered (L_o) and disordered (L_d) domains can be clearly identified in AFM imaging. We measured several other parameters also to test their correlation with F_X. The effect of 5 mM serotonin on the F_X of each of these bilayers could be measured with AFM. The detailed results for POPG and for the L_o and L_d domains of DEC221 are given in the supporting material (sections S2.1 and S2.2). In summary, for POPG membranes, the average F_X increases by 368% ± 158%. Nile Red spectra shift to shorter wavelengths with G/R value increasing from 0.34 ± 0.04 to 0.66 ± 0.05, representing a 94% ± 22% increase and implying a substantial increase of membrane order. However, there is no change observed in the NMR order parameter in the presence of serotonin (supporting material, section S2.1; Fig. S1).

For the biphasic DEC221 membrane, the average Fx decreases by 52.0% ± 8.3% and 32.0% ± 10.3% in the L_o and L_d phases, respectively. Nile Red spectra shift to a lower wavelength, and the G/R value increases from 0.78 ± 0.01 to 0.85 ± 0.05 in the presence of serotonin for the L_o phase (average G/R value increases by 9% ± 6%). For the L_d phase, the G/R value increases from 0.52 ± 0.01 to 0.59 ± 0.02 (average G/R value increases by 13% ± 4%), indicating minimal changes. However, the Laurdan GP value increases from −0.16 ± 0.01 to −0.06 ± 0.01 in the L_d phase and from 0.30 ± 0.05 to 0.42 ± 0.06 in the L_o phase. Thus, the average GP value for Laurdan increases substantially by 40% ± 27% and 63% ± 10% in the L_o and L_d phases, respectively. The average translational diffusion coefficient D_T, as measured by z-scan FCS, decreases from 5.4 ± 0.5 to 1.6 ± 0.1 $\mu m^2 s^{-1}$, indicating an average decrease in D_T by 70% ± 11% in the presence of 5 mM serotonin (supporting material, section S2.2; Fig. S2). In our previous studies, we have measured the NMR order parameter for a biphasic membrane system PEC221 (except DOPC in DEC221, this membrane contained POPC, which could be chain deuterated) in the absence and the presence of serotonin. The NMR order parameter decreased in the disordered phase and increased in the ordered phase in the presence of 9 mol % serotonin (46).

In order to compare the different measurements (which have different units), we have plotted a histogram of changes measured in units of standard deviation for each type of measurement (Fig. 2). In relative terms, this shows how significant the changes are. Fig. 2 *A* represents measurements made on PPC111, while Fig. 2 *B–D* represent measurements on POPG, DEC221 (L_d), and DEC 221 (L_o), respectively.

DISCUSSION

The term order of a membrane refers to a unifying concept that is assumed to characterize a host of properties of the bilayer. For example, a decrease in membrane order is expected to make it easier to produce a disruption in the membrane, rendering the acyl chains of the lipids more dynamic and the hydrophobic interior partially polar and consequently allowing more efficient diffusion of a probe into the membrane. Each of these properties can be measured with a set of different techniques. The change in membrane order upon the addition of a perturbant is expected to reflect in all these measurements, at least qualitatively. A few studies have validated this assumption, but they have compared only a few techniques (24,26,41,42). Here, we have employed a large variety of techniques (9 in total) to measure the change in the membrane order by small molecules known to modulate the membrane properties.

We have studied the effect of serotonin, a small lipophilic molecule known to modulate the membrane properties (25,46–48), on the model membrane mixture PPC111. Serotonin is an archetypal monoamine neurotransmitter that is known to have long-term neuromodulatory effects compared with typical neurotransmitters (51–53). A modulation of the membrane properties can be a putative pathway of its action (25). It is also packed at 100s of mM concentration in the vesicles (54) and therefore can have a significant

measurements). (*E–G*, *I*, and *J*) Calculation of the generalized polarization (GP) of Laurdan in supported phase-separated model membrane DEC221. (*E*) and (*I*) are images recorded in the green and blue regions. (*F*) and (*J*) are the images obtained with the indicated formula to generate images 3 and 4. (*G*) The GP image. (*K*) Schematic of the fluorescence spectral properties of Laurdan in ordered and disordered membrane environments. (*H*) Representative GP image of PPC111 SLB. (*L*) Representative GP image of PPC111 SLB in the presence of 5 mM serotonin. Scale bar: 10 μm. (*M*) GP value of Laurdan dye in the PPC111 bilayer in the absence (*black*) and presence (*red*) of 5 mM serotonin (average of $N = 3$ measurements). (*N* and *O*) Changes in the rotational anisotropy of DPH and TMA-DPH dyes in the PPC111 SLB with increasing concentrations of serotonin probed by steady-state anisotropy experiments. (*P*) A representative Raman spectrum (normalized at 2885 cm^{-1}) of the PPC111 SLB in the absence (*black*) and presence (*light brown*) of 20 mM serotonin. (*Q*) Relative change in the mean value of I_{2882}/I_{2845} and I_{2845}/I_{2923} of PPC111 bilayer in the presence of 20 mM serotonin (average of $N = 5$ measurements). (*R*) ^2H NMR order parameter along the deuterated lipid chains for POPC-d_{31} and POPG-d_{31} in the absence and presence of 10 mol % serotonin at 25°C (reproduced from Dey et al. (25)). Error bar represents mean ± SE.

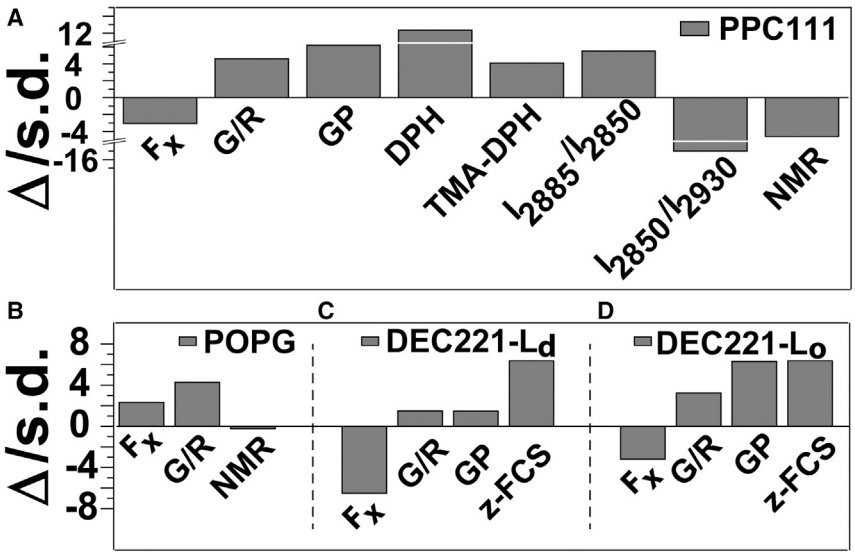

FIGURE 2 A comparison of measurements of serotonin-induced changes between different techniques. The changes are represented in units of the standard deviation of the measurements. Δ, change upon serotonin addition (after – before); s.d., standard deviation. (*A–D*) The figures represent measurements obtained from different techniques on PPC111 (*A*), POPG (*B*), disordered phase L_d of DEC221 (*C*), and ordered phase L_o of DEC221 (*D*). Positive change means order increases upon serotonin incubation.

effect on the membrane. So, its interaction with the lipid membrane assumes strong biological significance. We employed AFM force indentation (F_X), Nile Red fluorescence spectral studies (G/R), NMR order parameter (NMR), Laurdan GP (GP), DPH and TMA-DPH steady-state anisotropy, and ratiometric Raman spectroscopy of lipid modes (I_{2885}/I_{2850} and I_{2850}/I_{2930}). We note that the serotonin/lipid molar ratio is not the same for all the techniques employed. For a PPC111 vesicle at 5 mM serotonin, the partition coefficient is 1500, indicating that there is 11% serotonin/lipid molar ratio in the membrane (25). We add a note of caution that this is only an estimate, and this number can vary for a supported lipid bilayer. However, it shows that the molar ratios are of the same order of magnitude in the different experiments. In addition, we also note that the concentration of the perturbant is expected to govern the extent of change in the membrane order but not the direction of change. So, our main conclusion remains robust with respect to differences in the exact concentration of serotonin in different experiments. AFM force indentation, NMR order parameter, and Raman I_{2850}/I_{2930} ratio measurements suggest that the PPC111 membrane becomes more disordered upon incubation with serotonin (Fig. 2 *A*). However, Nile Red spectral shift in terms of the G/R ratio, Laurdan GP value, DPH and TMA-DPH anisotropy, and Raman I_{2885}/I_{2850} ratio measurements show that the PPC111 membrane becomes more ordered in the presence of serotonin.

All these results strongly suggest that different techniques may measure somewhat different properties of the membrane. However, we could still find the correlation between a subgroup of techniques, such as AFM and NMR. This raises the possibility that a specific group of techniques may always correlate with each other and thus could be placed under a common category.

This possibility is investigated by probing a different membrane composition, namely POPG. F_X and G/R measurements suggest that serotonin makes the POPG membrane more ordered (Fig. 2 *B*). However, NMR shows that serotonin does not alter the order of the POPG membrane. This is opposite to what we have observed in the case of the PPC111 membrane and shows that a given pair of techniques do not always correlate with one another.

We have also studied the effect of serotonin on the order of biphasic model membrane DEC221, which forms coexisting ordered and disordered phases. Each membrane phase has distinct membrane order, thus how different probes respond to these phases can be studied simultaneously on the same membrane. We found that different probes could differentiate between the mechanical properties of the two phases. However, F_X is anticorrelated with G/R, GP, and z-FCS measurements in both the phases (Fig. 2 *C* and *D*), so different techniques do not even agree between two neighboring phases on the same membrane.

Thus, we found a lack of universal correlation between different types of techniques, with no consistent rule predicting whether two types of techniques would correlate with each other. This lack of correlation is also observed for different membrane compositions, suggesting that our finding is not limited to a particular membrane mixture. Our study also highlights that the correlation found between a few techniques in the previous studies is probably a coincidence. For instance, there are studies that have shown the correlation of Laurdan GP with NMR order parameters (42) and AFM F_X measurements (26). But in our study on the PPC111 bilayer, both the techniques are anticorrelated with Laurdan GP measurements. While the reason for this is not clear right now, it is obvious that the assumption that all probes report a perturbation of the bilayer in a single consistent way is not correct. Different techniques mainly measure the membrane properties depending on the localization of the probes and on the temporal and spatial scales of the techniques. Thus, it is important to understand how

each of these parameters are related to a specific property of the membrane instead of implying that any of it is an average measurement of membrane order. It is worth noting that, as of now, our findings hold for the perturbant serotonin. We do not have proof that this discrepancy can be generalized beyond serotonin. However, we expect that the effect is more general. Any small molecule engaged in headgroup interactions similar to serotonin may lead to this response. We are currently carrying out measurements involving other neurotransmitters as well as other membrane-active molecules.

Finally, the issue of probe-related versus probe-free measurements of membrane order remains. We note that the direction of change measured by different fluorescence spectroscopy-based techniques are generally correlated, though their amplitudes are frequently not. For example, the Laurdan GP value shows only a small increase of membrane order in the disordered domain of DEC221 but a robust increase in the ordered domains (Fig. 2 *C* and *D*). On the other hand, z-FCS shows increase of similar magnitudes in both the phases. Although heavily debated ever since such measurements were introduced, it is agreed that bulky fluorescence probes may represent a local perturbation of lipid packing, while AFM and NMR techniques directly measure membrane order (neglecting isotope effects in NMR measurements). Clearly, molecular parameters such as probe amplitude, correlation time of motion, etc., are not comparable between the methods. Molecular order is not "static" but does depend on the time window over which motions are sampled. Lipid membranes are subject to complex dynamic landscapes and holistic concepts are required to fully describe membrane order and elasticity, typically involving the combination of several experimental and computational techniques (55). For instance, molecular dynamics simulations, Monte Carlo simulations, or theoretical modeling can be used to mimic the experimental response of a particular probe in the membranes. Such studies will improve our understanding of what exactly these probes are measuring in the membrane.

CONCLUSIONS

The lipid bilayer is characterized by the heterogeneous distribution of various lipid headgroups, acyl tails, and surface, interfacial, and percolated water in the acyl chain region. Individual as well as collective behavior of these different components generate lateral and *trans*-bilayer heterogeneity in terms of polarity, lateral and rotational diffusion of lipids, viscosity, and hydration of the membrane. All the techniques that are used to determine membrane order do not measure the same property of the membrane. For example, AFM F_X measurements directly determine the mechanical stability of the lipid bilayer, whereas fluorescence-based measurements are mostly dependent on the rotational flexibility and polarity of the lipidic microenvironment at the place where the probe is located. Therefore, it is perhaps not surprising that the membrane order parameters obtained from different techniques are not correlated. In conclusion, a generalized notion of membrane order is best avoided, and one must be cautious in drawing biological inferences from it. A correlation of relevant functions and membrane properties must first be established before drawing any inference from a particular measurement.

SUPPORTING MATERIAL

Supporting material can be found online at https://doi.org/10.1016/j.bpj.2022.08.029.

AUTHOR CONTRIBUTIONS

D.H. and S.M. designed experiments and conceptualized the study. A.G., M.K., D.S.R., O.E., and H.C. performed experiments and analyzed data. S.M. wrote article with input and contributions from all coauthors.

ACKNOWLEDGMENTS

We dedicate this study to Dr. Klaus Gawrisch, our mentor, friend, and most highly appreciated colleague. Membrane order is a topic that has always been inspired and much benefited from Klaus's seminal contributions. The scientific advice, encouragements, and critical and very constructive support throughout the last 30 years are highlighting his great contributions to membrane biophysics. D.H. thanks Klaus very personally for his friendship, support, help, and career advice; without you, Klaus, I would not be where I am.

This work was supported by the department of Atomic Energy, Goverment of India, provided under project no RTI4003. O.E. acknowledges support by the Magnus Ehrnrooth foundation, and Ruth and Nils-Erik Stenbäck's Foundation.

DECLARATION OF INTERESTS

The authors declare no competing interests.

REFERENCES

1. Bozelli, J. C., and R. M. Epand. 2020. Determinants of lipids acyl chain specificity: a tale of two enzymes. *Biophys. Chem.* 265:106431. https://doi.org/10.1016/J.BPC.2020.106431.
2. Cheng, X., and J. C. Smith. 2019. Biological membrane organization and cellular signaling. *Chem. Rev.* 119:5849–5880. https://doi.org/10.1021/acs.chemrev.8b00439.
3. Muller, M. P., T. Jiang, …, E. Tajkhorshid. 2019. Characterization of lipid-protein interactions and lipid-mediated modulation of membrane protein function through molecular simulation. *Chem. Rev.* 119:6086–6161. https://doi.org/10.1021/acs.chemrev.8b00608.
4. Faustino, I., H. Abdizadeh, …, S. J. Marrink. 2020. Membrane mediated toppling mechanism of the folate energy coupling factor transporter. *Nat. Commun.* 11:1763–1769. https://doi.org/10.1038/s41467-020-15554-9.
5. Bozelli, J. C., S. S. Aulakh, and R. M. Epand. 2021. Membrane shape as determinant of protein properties. *Biophys. Chem.* 273:106587. https://doi.org/10.1016/J.BPC.2021.106587.

6. Oseid, D. E., L. Song, …, A. S. Robinson. 2020. Nuclear translocation of the unliganded glucocorticoid receptor is influenced by membrane fluidity, but not A2AR agonism. *Steroids.* 160:108641. https://doi.org/10.1016/j.steroids.2020.108641.
7. Giacomello, M., A. Pyakurel, …, L. Scorrano. 2020. The cell biology of mitochondrial membrane dynamics. *Nat. Rev. Mol. Cell Biol.* 21:204–224. https://doi.org/10.1038/s41580-020-0210-7.
8. Zielińska, A., A. Savietto, …, D. J. Scheffers. 2020. Flotillin-mediated membrane fluidity controls peptidoglycan synthesis and MreB movement. *Elife.* 9. . e57179–21. https://doi.org/10.7554/ELIFE.57179.
9. Sastre, D. E., L. G. M. Basso, …, M. E. Guerin. 2020. Membrane fluidity adjusts the insertion of the transacylase PlsX to regulate phospholipid biosynthesis in gram-positive bacteria. *J. Biol. Chem.* 295:2136–2147. https://doi.org/10.1074/jbc.RA119.011122.
10. Lee, S. M., S. H. Lee, …, K. S. Kwon. 2020. FABP3-mediated membrane lipid saturation alters fluidity and induces ER stress in skeletal muscle with aging. *Nat. Commun.* 11:5661–5715. https://doi.org/10.1038/s41467-020-19501-6.
11. Gastaldo, I. P., H. V. Rheinstädter, and M. C. Rheinstädter. 2020. Perspective on the role of the physical properties of membranes in neurodegenerative and infectious diseases. *Appl. Phys. Lett.* 117:040501. https://doi.org/10.1063/5.0018709.
12. Bianchetti, G., L. Viti, …, G. Maulucci. 2021. Erythrocyte membrane fluidity as a marker of diabetic retinopathy in type 1 diabetes mellitus. *Eur. J. Clin. Invest.* 51. . e13455–6. https://doi.org/10.1111/eci.13455.
13. Dadhich, R., M. Mishra, …, S. Kapoor. 2020. A virulence-associated glycolipid with distinct conformational attributes: impact on lateral organization of host plasma membrane, autophagy, and signaling. *ACS Chem. Biol.* 15:740–750. https://doi.org/10.1021/acschembio.9b00991.
14. Bompard, J., A. Rosso, …, O. Maniti. 2020. Membrane fluidity as a new means to selectively target cancer cells with fusogenic lipid carriers. *Langmuir.* 36:5134–5144. https://doi.org/10.1021/acs.langmuir.0c00262.
15. Kucherak, O. A., S. Oncul, …, A. S. Klymchenko. 2010. Switchable Nile Red-based probe for cholesterol and lipid order at the outer leaflet of biomembranes. *J. Am. Chem. Soc.* 132:4907–4916. https://doi.org/10.1021/ja100351w.
16. Moon, S., R. Yan, …, K. Xu. 2017. Spectrally resolved, functional super-resolution microscopy reveals nanoscale compositional heterogeneity in live-cell membranes. *J. Am. Chem. Soc.* 139:10944–10947. https://doi.org/10.1021/jacs.7b03846.
17. Sanchez, S. A., M. A. Tricerri, and E. Gratton. 2012. Laurdan generalized polarization fluctuations measures membrane packing micro-heterogeneity in vivo. *Proc. Natl. Acad. Sci. USA.* 109:7314–7319. https://doi.org/10.1073/pnas.1118288109.
18. Kaiser, H. J., D. Lingwood, …, K. Simons. 2009. Order of lipid phases in model and plasma membranes. *Proc. Natl. Acad. Sci. USA.* 106:16645–16650. https://doi.org/10.1073/pnas.0908987106.
19. Halder, A., B. Saha, …, S. Karmakar. 2018. Lipid chain saturation and the cholesterol in the phospholipid membrane affect the spectroscopic Properties of lipophilic dye Nile Red. *Spectrochim. Acta Mol. Biomol. Spectrosc.* 191:104–110. https://doi.org/10.1016/j.saa.2017.10.002.
20. Parasassi, T., G. de Stasio, …, E. Gratton. 1991. Quantitation of lipid phases in phospholipid vesicles by the generalized polarization of Laurdan fluorescence. *Biophys. J.* 60:179–189. https://doi.org/10.1016/S0006-3495(91)82041-0.
21. Zhang, Y. L., J. A. Frangos, and M. Chachisvilis. 2006. Laurdan fluorescence senses mechanical strain in the lipid bilayer membrane. *Biochem. Biophys. Res. Commun.* 347:838–841. https://doi.org/10.1016/j.bbrc.2006.06.152.
22. Filipe, H. A. L., M. J. Moreno, and L. M. S. Loura. 2020. The secret lives of fluorescent membrane probes as revealed by molecular dynamics simulations. *Molecules.* 25:E3424–E3443. https://doi.org/10.3390/molecules25153424.
23. Sezgin, E., T. Sadowski, and K. Simons. 2014. Measuring lipid packing of model and cellular membranes with environment sensitive probes. *Langmuir.* 30:8160–8166. https://doi.org/10.1021/la501226v.
24. Moulton, E. R., K. J. Hirsche, …, J. D. Bell. 2018. Examining the effects of cholesterol on model membranes at high temperatures: Laurdan and Patman see it differently. *Biochim. Biophys. Acta Biomembr.* 1860:1571–1579. https://doi.org/10.1016/j.bbamem.2018.05.013.
25. Dey, S., D. Surendran, …, S. Maiti. 2021. Altered membrane mechanics provides a receptor-independent pathway for serotonin action. *Chemistry.* 27:7533–7541. https://doi.org/10.1002/chem.202100328.
26. Monasterio, B. G., N. Jiménez-Rojo, …, A. Alonso. 2020. Patches and blebs: a comparative study of the composition and biophysical properties of two plasma membrane preparations from CHO cells. *Int. J. Mol. Sci.* 21:26433–E2711. https://doi.org/10.3390/ijms21072643.
27. Sengupta, P., J. Balaji, and S. Maiti. 2002. Measuring diffusion in cell membranes by fluorescence correlation spectroscopy. *Methods.* 27:374–387. https://doi.org/10.1016/S1046-2023(02)00096-8.
28. Steinberger, T., R. Macháň, and M. Hof. 2014. Z-scan fluorescence correlation spectroscopy as a Ttool for diffusion measurements in planar lipid membranes. *Methods Mol. Biol.* 1076:617–634. https://doi.org/10.1007/978-1-62703-649-8_28.
29. Wallach, D. F., S. P. Verma, and J. Fookson. 1979. Application of laser Raman and infrared spectroscopy to the analysis of membrane structure. *Biochim. Biophys. Acta Rev. Biomembr.* 559:153–208. https://doi.org/10.1016/0304-4157(79)90001-7.
30. Gaber, B. P., and W. L. Peticolas. 1977. On the quantitative interpretation of biomembrane structure by Raman spectroscopy. *Biochim. Biophys. Acta.* 465:260–274. https://doi.org/10.1016/0005-2736(77)90078-5.
31. Davis, J. H. 1983. The description of membrane lipid conformation, drder and dynamics by 2H-NMR. *Biochim. Biophys. Acta.* 737:117–171. https://doi.org/10.1016/0304-4157(83)90015-1.
32. Molugu, T. R., S. Lee, …, M. F. Brown. 2017. Concepts and methods of solid-state NMR spectroscopy applied to biomembranes. *Chem. Rev.* 117:12087–12132. https://doi.org/10.1021/acs.chemrev.6b00619.
33. Huster, D., K. Arnold, and K. Gawrisch. 1998. Influence of docosahexaenoic acid and cholesterol on lateral lipid organization in phospholipid mixtures. *Biochemistry.* 37:17299–17308. https://doi.org/10.1021/bi980078g.
34. Leftin, A., T. R. Molugu, C. Job, K. Beyer, and M. F. Brown. 2014. Area per lipid and cholesterol interactions in membranes from separated local-field 13C NMR spectroscopy. *Biophys. J.* 107:2274–2286. https://doi.org/10.1016/J.BPJ.2014.07.044.
35. Ferreira, T. M., F. Coreta-Gomes, …, D. Topgaard. 2013. Cholesterol and POPC segmental order parameters in lipid membranes: solid state 1H–13C NMR and MD simulation studies. *Phys. Chem. Chem. Phys.* 15:1976–1989. https://doi.org/10.1039/C2CP42738A.
36. Hassan-Zadeh, E., F. Hussain, and J. Huang. 2017. Gramicidin peptides alter global lipid compositions and bilayer thicknesses of coexisting liquid-ordered and liquid-disordered membrane domains. *Langmuir.* 33:3324–3332. https://doi.org/10.1021/acs.langmuir.6b03688.
37. Gaus, K., S. Le Lay, …, M. A. Schwartz. 2006. Integrin-mediated adhesion regulates membrane order. *J. Cell Biol.* 174:725–734. https://doi.org/10.1083/jcb.200603034.
38. Zorilă, B., G. Necula, …, M. Bacalum. 2020. Melittin induces local order changes in artificial and biological membranes as revealed by spectral analysis of Laurdan fluorescence. *Toxins.* 12:1210705. https://doi.org/10.3390/toxins12110705.
39. Bernardes, N., A. R. Garizo, …, A. M. Fialho. 2018. Azurin interaction with the lipid raft components ganglioside GM-1 and caveolin-1 increases membrane fluidity and sensitivity to anti-cancer drugs. *Cell Cycle.* 17:1649–1666. https://doi.org/10.1080/15384101.2018.1489178.
40. Lorizate, M., B. Brügger, …, H. G. Kräusslich. 2009. Probing HIV-1 membrane liquid order by Laurdan staining reveals producer cell-dependent differences. *J. Biol. Chem.* 284:22238–22247. https://doi.org/10.1074/jbc.M109.029256.
41. Steinkühler, J., E. Sezgin, …, R. Dimova. 2019. Mechanical properties of plasma membrane vesicles correlate with lipid order, viscosity and cell density. *Commun. Biol.* 2:337–338. https://doi.org/10.1038/s42003-019-0583-3.

42. Leung, S. S. W., J. Brewer, …, J. L. Thewalt. 2019. Measuring molecular order for lipid membrane phase studies: linear relationship between Laurdan generalized polarization and deuterium NMR order parameter. *Biochim. Biophys. Acta Biomembr.* 1861:183053. https://doi.org/10.1016/j.bbamem.2019.183053.

43. Postila, P. A., and T. Róg. 2020. A perspective: active role of lipids in neurotransmitter dynamics. *Mol. Neurobiol.* 57:910–925. https://doi.org/10.1007/s12035-019-01775-7.

44. Peters, G. H., C. Wang, …, P. Westh. 2013. Binding of serotonin to lipid membranes. *J. Am. Chem. Soc.* 135:2164–2171. https://doi.org/10.1021/ja306681d.

45. Josey, B. P., F. Heinrich, …, M. Lösche. 2020. Association of model neurotransmitters with lipid bilayer membranes. *Biophys. J.* 118:1044–1057. https://doi.org/10.1016/j.bpj.2020.01.016.

46. Engberg, O., A. Bochicchio, …, D. Huster. 2020. Serotonin alters the phase equilibrium of a ternary mixture of phospholipids and cholesterol. *Front. Physiol.* 11:578868–578914. https://doi.org/10.3389/fphys.2020.578868.

47. Bochicchio, A., A. F. Brandner, …, R. A. Böckmann. 2020. Spontaneous membrane nanodomain formation in the absence or presence of the neurotransmitter serotonin. *Front. Cell Dev. Biol.* 8:601145–601217. https://doi.org/10.3389/fcell.2020.601145.

48. Musabirova, G., O. Engberg, …, D. Huster. 2022. Serotonergic drugs modulate the phase behavior of complex lipid bilayers. *Biochimie*, . In press. https://doi.org/10.1016/j.biochi.2022.04.006.

49. Leonenko, Z. V., A. Carnini, and D. T. Cramb. 2000. Supported planar bilayer formation by vesicle fusion: the interaction of phospholipid vesicles with surfaces and the effect of gramicidin on bilayer properties using atomic force microscopy. *Biochim. Biophys. Acta.* 1509:131–147. https://doi.org/10.1016/S0005-2736(00)00288-1.

50. Kaiser, R. D., and E. London. 1998. Location of diphenylhexatriene (DPH) and its derivatives within membranes: comparison of different fluorescence quenching analyses of membrane depth. *Biochemistry.* 37:8180–8190. https://doi.org/10.1021/bi980064a.

51. Coray, R., and B. B. Quednow. 2022. The role of serotonin in declarative memory: a systematic review of animal and human research. *Neurosci. Biobehav. Rev.* 139:104729. https://doi.org/10.1016/j.neubiorev.2022.104729.

52. Murano, M., F. Saitow, and H. Suzuki. 2011. Modulatory effects of serotonin on glutamatergic synaptic transmission and long-term depression in the deep cerebellar nuclei. *Neuroscience.* 172:118–128. https://doi.org/10.1016/j.neuroscience.2010.10.037.

53. Hirono, M., F. Karube, and Y. Yanagawa. 2021. Modulatory effects of monoamines and perineuronal nets on output of cerebellar purkinje cells. *Front. Neural Circ.* 15:661899. https://doi.org/10.3389/fncir.2021.661899.

54. Balaji, J., R. Desai, …, S. Maiti. 2005. Quantitative measurement of serotonin synthesis and sequestration in individual live neuronal cells. *J. Neurochem.* 95:1217–1226. https://doi.org/10.1111/j.1471-4159.2005.03489.x.

55. Smith, A. A., A. Vogel, …, D. Huster. 2022. A method to construct the dynamic landscape of a bio-membrane with experiment and simulation. *Nat. Commun.* 13:108. https://doi.org/10.1038/s41467-021-27417-y.

Biophysical Journal, Volume *122*

Supplemental information

Different membrane order measurement techniques are not mutually consistent

Ankur Gupta, Mamata Kallianpur, Debsankar Saha Roy, Oskar Engberg, Hirak Chakrabarty, Daniel Huster, and Sudipta Maiti

Supplementary Information

Different Membrane Order Measurement Techniques are Not Mutually Consistent

Ankur Gupta#, Mamata Kallianpur#, Debsankar Saha Roy#, Oskar Engberg$, Hirak Chakrabarty^, Daniel Huster$#*, and Sudipta Maiti#*

1. Materials and Methods

The lipids POPC (16:0-18:1 PC), POPG (16:0-18:1 PG), DOPC (18:1 (Δ9-Cis) PC), Egg-sphingomyelin, 1,2-dioleoyl-*sn*-glycero-3-phosphoethanolamine-N (lissamine rhodamine B sulfonyl) (18:1 Liss Rhod PE), Lipid extruding kit, 10 mm Filter Supports, Nucleopore Track-etched polycarbonate membrane (pore diameter 50 nm) were purchased from Avanti Polar Lipids Inc. (Alabaster, USA). Cholesterol and methyl-β-cyclodextrin (mβCD) were purchased from Sigma Aldrich (St. Louis, MO). Serotonin-hydrochloride was purchased from Merck (Darmstadt, Germany). Sodium chloride and calcium chloride dehydrate were purchased from Merck Life Science Private Limited (India). Chloroform and methanol AR graded were purchased from S. D. Fine Chemical Ltd. (India). All the chemicals were used without any additional purification. Supported bilayers were formed on mica (grade V4 muscovite) as support purchased from SPI supplies (West Chester, USA). All the experiments were performed using milli-Q water (conductivity18.2 MΩ cm^{-1}) obtained from a Milli-Q gradient system (Millipore, Germany).

1.1. Preparation of supported bilayers

The mica supported lipid bilayer (SLB) was prepared by following the vesicle fusion method.[1] Two monophasic bilayers - pure POPG and POPC/POPG/cholesterol in the molar ratio of 1/1/1 (PPC111) were prepared by weighing the powders in the respective molar ratio and dissolving them in the chloroform solvent. To prepare a biphasic phase-separated bilayer, lipids DOPC/Egg SM/cholesterol in the molar ratio of 2/2/1/ (DEC221) were weighed and dissolved in the 1/1 (by volume) chloroform/methanol solvents. The solvent was then evaporated by purging iolar argon gas to make a dried film called lipid film. The dried lipid film was kept in a vacuum desiccator for ~24 hours to completely remove organic solvents which were then rehydrated using either milli-Q water or buffer (150 mM NaCl) to make a lipid suspension of concentration 2.5 mg/mL. The solution was vortexed properly for ~10 minutes to form multilamellar vesicles (MLVs). The MLVs were passed through an extruder (Avanti Polar Lipids Inc., Alabaster) containing a polycarbonate membrane of 50 nm pore size (covered by two 10 mm filter supports on each side of the membrane) using 1000 µL vacuum-sealed syringes (Hamilton, Avanti Polar lipids Inc.) to obtain a clear solution containing uniform small unilamellar vesicles (SUVs). The extrusion was performed at 60°C. Bilayer was formed by adding 40 µL of 100 mM calcium chloride solution, 50 µL of SUVs, and 210 µL of water (or buffer) together (all were preheated to 65ºC in a water bath) on a freshly cleaved mica glued to a glass petri dish and keeping it in a water bath at 70°C for 1 hour. The vesicles fuse to form a bilayer in this condition. The excess unfused vesicles were removed by thoroughly rinsing the bilayer with water or buffer. The formation of lipid

bilayer was confirmed by the AFM force indentation study. The buffer composition is 145 mM NaCl, 5.4 mM KCl, 20 mM Na-HEPES, and pH 7.4.

1.2. AFM Force Indentation

All AFM measurements were recorded using the commercial NanoWizard II system (JPK Instruments, Berlin, Germany). The AFM instrument was mounted on an Axiovert Inverted Microscope (Zeiss, Germany). The calibration of sensitivity, resonance frequencies (both in air and in water), and determination of the spring constant was done before each force experiment using the thermal noise method.[2] The cantilever used for all the force experiments has a resonance frequency of 10-20 kHz and a spring constant of 0.03 N/m. Sensitivity and spring constant measurements were also performed after the end of each experiment. The sensitivity values were similar before and after the experiments within errors. All the AFM force experiments were performed on the supported bilayers which were formed on mica glued to coverslip glass in a liquid cell. The bilayer remained hydrated until the end of the experiment.

For all the bilayer force experiments, the total Z piezo displacement was 1.0 μm. The piezo velocity both for approach and retraction was kept at 0.5 $\mu m \cdot s^{-1}$. In the AFM force indentation study, a sharp AFM tip is brought to the SLBs from the top. The force remained zero when the tip is away from the top surface of the bilayer in the non-contact region (Figure 1A, a to b part of curve). As soon as the AFM tip hit the surface of the bilayer at the contact point, the force starts increasing. The tip continues to approach and indent into the membrane with increasing force (Figure 1A, b to c part of curve) till the membrane rupture locally. This rupturing of the membrane is characterized by a 'kink' in the force vs tip z-displacement curve (Figure 1A, point c on the curve). After that, the tip approaches the hard mica surface and the force continues to increase till it reaches the force value set by us (Figure 1A, d to e part of curve). The force value corresponding to this 'kink' is known as the breakthrough force (F_X) or the indentation force and it is the measure of the stiffness of the membrane. In general, stiffness is assumed to be proportional to the order of the membrane. So, the higher the stiffness of the membrane, the more ordered is the membrane. All the force experiments were carried out at different points on the bilayer. For each set, usually, 400-600 force curves were recorded. The force indentation curves were processed and analyzed using JPK Data Processing software. The breakthrough force values were extracted from each approach curve to build the histogram. The serotonin is incubated for 45 minutes for all the AFM experiments.

1.3. Spectral imaging of Nile red dye

The fluorescence spectra of supported bilayer bound Nile Red dye were obtained by performing confocal imaging in the lambda stacking mode on the commercial LSM 880. For lambda-stacking imaging, 514 nm excitation light was taken from an Ar++ laser, reflected by a dichroic mirror (MBS 514) and focused through a Zeiss C-Apochromat 40x, NA 1.2, water immersion objective onto the sample. The fluorescence emission was collected by the same objective and sent to the GaAsP detector through the monochromator with a resolution of 5 nm. Lambda stacks were independently acquired from 529 to 714 nm at the interval of 5 nm using an LSM 880 microscope (Carl Zeiss, Jena, Germany) with Zen imaging software. All the lambda imaging was done on the supported bilayers which were formed on the freshly cleaved mica already glued to coverslip glass in a Petri dish. Nile Red was incubated to SLBs with a concentration of ~ 1 μM for 20 minutes and the bilayer is washed to remove unbound Nile red as much as possible. The stock of Nile red was made in pure methanol and stored at

4^0C for further use. The serotonin is incubated for 45 minutes for all the experiments. The nature and peak of the fluorescence spectra of Nile red are sensitive to the packing of the lipids. If we compare the fluorescence spectra of dye in the aqueous environment (Figure 1C, orange cartoon spectra), disordered membrane environment (Figure 1C, green cartoon spectra) and ordered membrane environment (Figure 1C, blue cartoon spectra), the spectra have relatively more contribution of lower wavelength in the ordered membrane environment compared to disordered membrane environment.

1.4. Spectral Imaging of Laurdan

The multiphoton excitation of Laurdan is carried out on a modified confocal microscope (LSM 710, Carl Zeiss), which we have adapted for multiphoton excitation. Additionally, to enable us to use specific UV sensitive photomultiplier tubes (Electron Tubes, model: P30A-01, Electron Tubes Limited, UK) in the non-descanned path, we got two external additional signal input channels custom-made by the manufacturer. A Ti: sapphire laser (MaiTai DeepSee, Spectra-Physics) operating at 780 nm wavelength and producing ∼100 fs pulses (repetition rate = 80 MHz) is used for multi-photon excitation of Laurdan, with the DeepSee chirp compensator adjusted for maximum signal. Our custom-built multi-photon microscopy setup uses relatively low laser powers (27−30 mW at the back aperture). The fluorescence signal is collected in the epifluorescence mode. The emission is sent to the non-descanned channel after the backscattered excitation light is separated from the Laurdan fluorescence by a dichroic mirror (690+, part of LSM 710, Carl Zeiss) in the fluorescence turret. The Laurdan fluorescence in the ordered membrane environment is bluer shifted in wavelength compared to the disordered membrane environment as shown in Figure 1K. The Laurdan fluorescence spectrum has a peak centred at ~ 425 nm for the ordered membrane environment and ~500 nm for the disordered membrane environment. So, a 50/50 dichroic beam-splitter is used to split the fluorescence signal of Laurdan into two channels- the blue channel and the green channel. The blue channel fluorescence was collected through the filter 425/30 (bandwidth of 410-440 nm) and green channel fluorescence was collected through the filter 500/30 (bandwidth of 485-515 nm). These signals are detected by two analog photomultiplier tubes (PMTs, model: P30A-01, Electron Tubes Limited, UK). All the settings such as detector gain, laser power, etc. kept the same during the experiment. All the multiphoton imaging was done on the SLBs which were formed on the freshly cleaved mica already glued to coverslip glass in a Petri dish. Laurdan was incubated to SLBs with a concentration of ~ 10 μM for 40 minutes and the bilayer is washed to remove unbound Laurdan as much as possible. The 1 mM stock of Laurdan was made in pure DMSO and stored at 4°C for further use. To quantify the order of the membrane by Laurdan dye, the Generalized Polarization (GP) of the membrane is calculated using equation 1. The complete flowchart to calculate the GP value from the obtained blue and green channel images is shown in Figure 1 (E to L). The representative membrane system in the flowchart is the phase-separated DEC221 SLB. This SLB has coexisting ordered and disordered phases at room temperature. The green channel (485-515 nm) and blue channel (410-440 nm) images are shown in Figures 1E and 1I respectively. The intensity image of both channels is computed in the ImageJ software and both the images are added (Figure 1F) and subtracted (Figure 1J) performing image arithmetic in ImageJ according to equation 1 to get the final GP image (Figure 1G). Then the average GP value is calculated from the GP image. The GP value for the monophasic bilayer such as the PPC111 bilayer is calculated simply by calculating the average GP of the whole image. But for phase-separated bilayers such as DEC221, GP for specific phases is calculated by selecting ROI separately for each phase and taking the average GP of the ROI.

$$GP = \frac{\text{Intensity of blue channel} - (G * \text{Intensity of green channel})}{\text{Intensity of blue channel} + (G * \text{Intensity of green channel})} \quad (1)$$

The G-factor is calculated by taking fluorescence measurement of Laurdan dye in pure DMSO in a commercial spectrofluorimeter Fluorolog 3 (Horiba, Jobin Yvon). The excitation wavelength was set to 385 nm and emission was collected from the 400-600 nm range. The fluorescence emission was separated into blue (average intensity from 410-440 nm) and green (average intensity from 485-515 nm) channels and the GP value was calculated from equation 1 by keeping G = 1. The obtained GP value was used to calculate G-factor. The same Laurdan dye in pure DMSO solution is used in the multiphoton imaging setup and intensity of blue and green channels are obtained. Now, the obtained GP value from the spectrofluorimeter and intensity of both channels in the multiphoton setup is put in equation 1 to obtain the G-factor. This G-factor was used to calculate the GP value of Laurdan in the supported bilayers. This calibration was done before each experiment.

1.5. Z-scan Fluorescence Correlation Spectroscopy (z-FCS) measurements

Z-scan FCS measurements were done on a home built combined AFM-confocal setup as described in.[3] Briefly, the expanded pulsed 543 nm laser from a supercontinuum laser source was guided by the help of reflecting and dichroic mirrors and focused into the sample using an apochromatic 60× water immersion objective with the numerical aperture of 1.2 (Olympus, PA, USA). The objective was mounted in a microscope (Axiovert 100M, Germany). The fluorescence signal obtained from the sample was collected from the same objective and was passed through the filters and focused onto a 25 µm core diameter optical fibre using a 160 mm positive lens (tube lens) mounted in the microscope. This optical fibre acts as a confocal pinhole to eliminate the out-of-focus fluorescence photons. The fluorescence photons were detected by a single-photon avalanche photodiode (APD, PerkinElmer Inc., Waltham, MA, USA). The APD signal was read by a hardware correlator present in the Picoharp300 module. The time traces of fluorescence intensity as a function of time were recorded using a correlator and Symphotime 32 software is used to calculate the raw autocorrelation function. The autocorrelation curves were recorded at different z-interval (along the bilayer axis) and at various xy coordinates in the sample by using an automated sample scanner (TAO-piezo scanner, Nanowizard II, JPK Instruments AG, Germany). The sample scanner was kept at a particular xy point and autocorrelation curves were recorded at different z-intervals by moving the scanner along the z-axis.
To perform the z-FCS measurements in the supported bilayers, the 18:1 Liss Rh PE was added with 0.05 mol% to the lipid mixture of the given molar ratio during lipid film preparation. All z-FCS experiments were done on the supported bilayers. The 5 mM serotonin is incubated for 45 minutes and the same points in the membrane are measured after serotonin addition.

The raw autocorrelation curves at each z were fitted with equation (2) in Origin 7.5 software (OriginLab, Northampton, MA, USA) to measure characteristic diffusion times τ_{D1} and τ_{D2} for the two components, amplitudes g_1 and g_2 of both diffusing components, triplet state fraction f and triplet state lifetime τ_1 of the dye and the background level bl. The autocorrelation curve is fitted with two diffusion components as there could be traces of unfused free vesicles in the bulk solution. The longer diffusion time is considered for further analysis as it is coming due to the diffusion of lipids in the supported bilayer. The diffusion

times at all z-interval were fitted with equation (5) to obtain the diffusion coefficient D_T value of lipids in the supported lipid bilayers.

(2) $G(\tau) = \left(\frac{1-f+f*e^{-\frac{t}{\tau_1}}}{1-f}\right) * \sum_{i=1}^{2}\left[\frac{g_i}{1+\frac{t}{\tau_{Di}}}\right] + bl$

(3) $\tau_D = \left(\frac{w^2}{4*D}\right)$

(4) $w^2 = \left(w_0^2\right)\left(1 + \frac{\lambda^2(\Delta z)^2}{\pi^2 n^2 w_0^4}\right)$

(5) $\tau_D = \left(\frac{w_0^2}{4*D}\right)\left(1 + \frac{\lambda^2(\Delta z)^2}{\pi^2 n^2 w_0^4}\right)$

w_0 = beam waist at focus, D_T = diffusion coefficient, λ = wavelength of light = 543 nm, n = refractive index of the medium = 1.33, z = axial distance, G (τ) = auto correlation function

1.6. Line-Confocal Raman Spectroscopy- Instrumentation and Data Analysis

Raman spectra were obtained with a home-built line-confocal Raman microscope as line-confocal excitation has ~ 11 times more signal-to-noise ratio compared to point-confocal and provides better sensitivity even at relatively low power leading to less photodamage of the biological samples.[4] The instrumental details are previously been described in.[4] Briefly, Raman spectra were recorded using 350 mW (at the back aperture of the objective lens) of a commercially sourced 532 nm laser beam (Verdi-V10, Coherent, USA). The laser was used for the line excitation to the bilayer sample where the line was created using a cylindrical lens, and focused by a 60× water objective (N.A. 1.2). The scattered light coming from the sample was collected by the same objective lens and separated by a 532 nm ultra-steep long-pass edge filter (LP0- 532RE-25, Semrock), and then, focused at the line slit of 300 μm of an imaging spectrometer (Horiba iHR320, Japan) and finally detected on the rectangular chip of the CCD camera (Synapse, Model No. 354308, Horiba, Japan). All the experiments were performed at room temperature. Each spectrum was acquired between 2650 and 3050 cm^{-1} (ν(C-H) region) with an integration time of 4 s and a total acquisition time of 13 minutes. The Raman spectra of this region of the membrane contain information about the order of the membrane (67-70). Intensities of scattered light were measured in increments of 0.018 nm (~0.5 cm^{-1}). From each acquired bilayer Raman spectrum, first, the water Raman spectrum was subtracted. After obtaining the subtracted spectrum, a linear baseline was fitted between 2650 and 3050 cm^{-1} and then subtracted to obtain the final spectrum. This spectrum was normalized to unity intensity at a 2885 cm^{-1} peak. The band intensities at 2850, 2885 and 2930 cm^{-1} were calculated as the maximum of the intensity nearest to the respective wavenumber. The spectra were smoothed using the Savitzy-Golay method (five data points, second-order polynomial). We have then measured the ratios of intensities I_{2885}/I_{2850} and I_{2850}/I_{2930} as these ratios are related to the order of the membrane. In general, the higher the value of the I_{2885}/I_{2850} ratio, the more is the coupling between the lipid chains and thus, the more ordered is the membrane. The higher the value of the I_{2850}/I_{2930} ratio, the lesser will be

the rotational freedom of the terminal methyl group in the lipid chains and thus, the more ordered is the membrane. We have measured the effect of serotonin on these two parameters of the model SLBs using Line-Confocal Raman spectroscopy. The serotonin is incubated for 45 minutes to obtain changes in the Raman peaks for all the experiments.

1.7. Steady-state anisotropy measurements

Steady-state fluorescence anisotropy measurements of DPH and TMA-DPH in membranes were carried out using Hitachi F-7000 (Japan) spectrofluorometer. Fluorescence anisotropy values were calculated using the following equation:

$$r = \frac{I_{VV} - GI_{VH}}{I_{VV} + 2GI_{VH}} \quad (6)$$

where $G = I_{HV}/I_{HH,}$ (grating correction or G-factor), I_{VV} and I_{VH} are the measured fluorescence intensities with the excitation polarizer vertically oriented, and the emission polarizer vertically and horizontally oriented, respectively. Both TMA-DPH and DPH were excited at 360 nm and their corresponding emission was monitored at 430 nm.

1.8. ^{2}H NMR measurements

Lipids were dissolved in 1:1 MeOH: chloroform and serotonin were dissolved in MeOH and co-dissolved for the serotonin-containing samples. To obtain a dry sample, the solvents were evaporated in a rotary evaporator at a 40°C water bath. To acquire a fluffy powder, the samples were re-dissolved in cyclohexane and lyophilized overnight at a high vacuum. Subsequently, the samples were hydrated with 50%wt HEPES buffer (20 mM HEPES, 0.1 mM EGTA, 150 mM NaCl). 10 freeze-thaw cycles between liquid nitrogen and a 40°C water bath were performed to produce multilamellar vesicles. To provide an inert environment for measurements, the samples were then inserted into 4 mm NMR rotors.

^{2}H NMR spectra were measured on a Bruker 750 Avance I NMR spectrometer at a resonance frequency of 115.1 MHz. A 5 mm double-channel solids probe was used. A phase-cycled quadrupolar echo sequence was used for signal acquisition[5] with a 30 µs delay between two π/2 pulses of 2.5-4 µs length. The spectral width was 500 kHz. The temperature of 25°C was used for all measurements. All NMR parameters were calculated using programs written in Mathcad software, as previously described.[6] To calculate the order parameters, the ^{2}H NMR spectrum was first dePaked to obtain smoothed order parameters as described in.[7] The NMR order parameter is obtained by one measurement. The standard deviation is assumed to be 3 times of the sensitivity of measurement (which is 0.001 unit).

2. Effect of serotonin on the 'membrane order' of model membrane

2.1. Serotonin induced perturbation of POPG membrane

The effect of serotonin on the POPG membrane is probed using AFM force indentation, Nile red spectral imaging and NMR order parameter.

2.1.1. AFM force indentation- We have measured the F_X of POPG SLB in the absence and presence of 5 mM serotonin using AFM force indentation. Figure S1A shows the representative histograms of F_X of POPG in the absence (black) and presence (red) of 5 mM serotonin. The histogram shows that F_X of the POPG bilayer increases in the presence of serotonin. The average F_X (% increase in force = [Average F_X of POPG bilayer in 5 mM serotonin - Average F_X of POPG bilayer in 0 mM serotonin] * [100/ Average F_X of POPG bilayer in 0 mM serotonin]) increases by (368 ± 158) % (Figure S1B), suggesting that POPG bilayer becomes more ordered in the presence of 5mM serotonin.

2.1.2. Spectral imaging of Nile Red- We have then measured the Nile red fluorescence spectra bound to POPG SLB in the absence (Figure S1C, black curve) and the presence of 5 mM serotonin (Figure S1C, red curve). The serotonin containing membranes has clearly blue-shifted fluorescence spectra compared to that without serotonin. The average G/R ratios in the absence and presence of serotonin are (0.34 ± 0.04) to (0.66 ±, 0.05) respectively, showing an increase of (94 ± 22) % in the average G/R value. This suggests that the POPG membrane becomes more ordered after 5mM serotonin addition.

2.1.3. Solid-State NMR- We have also measured the order parameter of the POPG vesicles in the absence and presence of 10 mol% serotonin using solid-state NMR (Figure S1D). The NMR measurement has shown that the order parameter of the POPG bilayer along the lipid acyl chain does not change in the presence of serotonin (Figure S1D and S1E), suggesting that the order of the POPG membrane is not altered by serotonin.

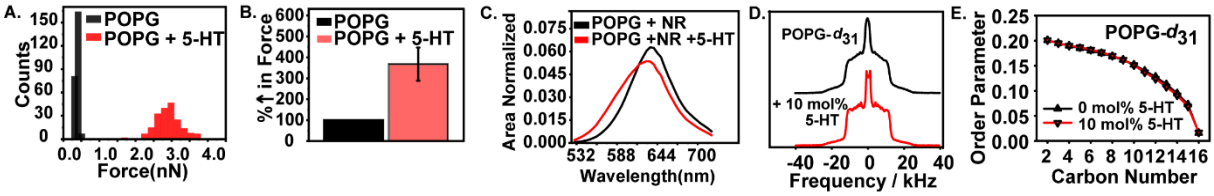

Figure S1. Effect of serotonin on the mechanical properties of POPG bilayer probed by different techniques. (A) A representative histogram of F_X on the POPG bilayer in the absence (black) and presence (red) of 5 mM serotonin. (B) Relative change in the average value of the F_X of POPG bilayer in the absence (black) and presence (red) of 5 mM serotonin (average of N = 4 measurements). (C) The fluorescence spectra of membrane-bound Nile Red dye in the POPG bilayer in the absence (black) and presence (red) of 5 mM serotonin (average of N = 3 measurements). (D) ^{2}H NMR spectra of POPG-d_{31} in the absence and presence of 10 mol% serotonin. (E) The ^{2}H NMR order parameter along the deuterated lipid chains for POPG- d_{31} in the absence and presence of 10 mol% serotonin. Error bar is S.E.M. All experiments are carried out in the buffer.

2.2. Serotonin induced perturbation of phase-separated DEC221 membrane

Here, we probed the effect of serotonin on the biphasic model membrane DEC221 using AFM force indentation, Nile red, Laurdan and FCS techniques.

2.2.1. AFM force indentation- DEC221 at room temperature phase separates to form ordered and disordered phases. The phases are visualized by AFM imaging.[8] In our previous study[8], we have measured the F_X of ordered and disordered phases separately in the absence and presence of 5 mM serotonin using AFM force indentation. Figures S2A and S2B (reproduced from Dey et al.[8]) show the representative histograms of F_X of disordered and ordered phases of DEC221 in the absence (black) and presence (red) of 5 mM serotonin. The histograms show that F_X of both the phases of the DEC221 bilayer decrease in the presence of serotonin. The average F_X are quantified for both the phases in the absence and presence of serotonin in Figure S2C (reproduced from Dey et al.[8]). The average F_X of the ordered phase is higher than the disordered phase by ~ 92 %. This clearly says that ordered phases are stiffer than disordered phases. The average F_X decrease both in the ordered as well as disordered phases in the presence of 5 mM serotonin (Figure S2A and S2B) by (52.0 ± 8.3) % and (32.0 ± 10.3) % respectively (Figure S2C), suggesting that serotonin makes both the membrane phases more disordered.

2.2.2. Spectral imaging of Nile Red- We have measured the serotonin-induced change in the fluorescence spectra of Nile red bound to DEC221 bilayer separately in ordered and disordered phases. We find that Nile Red has a preference for the disordered phase compared to the ordered phase by doing simultaneous AFM-confocal imaging of DEC221 incubated with Nile red. In this case, membrane phases are probed by AFM (Figure S2D) and fluorescence of Nile red is probed by confocal (Figure S2E) simultaneously by a home built combined AFM-confocal set-up (setup explained in our published work[3]), and by combining both the AFM and confocal images, phase-specific binding of Nile red is determined. We find that Nile red dye has ~ 4 times more binding in the disordered phase compared to the ordered phase. This preference resulted in the intensity contrast in the fluorescence confocal image. Because of this contrast, we are able to extract fluorescence spectra specific to ordered and disordered phases separately from the spectral image. The fluorescence spectra of Nile red in the disordered and ordered phases in the absence (Figure S2F and S2G, black curves) and the presence of 5 mM serotonin (Figure S2F and S2G, red curves) are shown respectively. The spectrum of Nile red in the ordered phase has more contribution of lower wavelength compared to the disordered phase and fluorescence peak in the ordered phase is ~8 nm shifted to lower wavelength compared to disordered phase (Figure S2F and S2G, black curves). This suggests that the ordered phase in fact is more ordered compared to the disordered phase. The serotonin containing membrane has a ~ 5 nm shift towards a lower wavelength with G/R increases from (0.78 ± 0.01) to (0.85 ± 0.05) for the ordered phase (average G/R value increases by (9 ± 6) %). There is no significant shift in the peak maxima of Nile red spectra in the presence of serotonin for the disordered phases. The G/R value increases from (0.52 ± 0.01) to (0.59 ± 0.02) by serotonin (average G/R value increases by (13 ± 4) %). This suggests that both the phases become more ordered after 5 mM serotonin addition.

2.2.3. Spectral imaging of Laurdan- The multiphoton imaging of the Laurdan dye bound to the DEC221 bilayer is performed. The average GP value of the disordered and ordered phases of DEC221 bilayer in the absence (Figure S2H and S2I, black bars) and presence (Figure S2H and S2I, red bars) of 5 mM serotonin is calculated respectively. We find that the GP value of ordered phases is higher than the disordered phases (S2H, S2I, black bars). This suggests that the ordered phases are indeed more ordered than the disordered phases. We further find that the Laurdan GP value increases from (-0.16 ± 0.01) to (-0.06 ± 0.01) in the disordered phase and from (0.30 ± 0.05) to (0.42 ± 0.06) in the ordered phase. The average

GP value increases by (40 ± 27) % (Figure S2I) and (63 ± 10) % (Figure S2H) in the ordered and disordered phases respectively. The increase in GP indicates that both the phases in DEC221 become more ordered in the presence of serotonin.

2.2.4. Z-FCS measurements- We have also looked at how the diffusion properties of lipids in the DEC221 bilayer are changed by serotonin. We have measured the diffusion coefficients of 0.5 mol% Liss Rhod PE doped DEC221 by z-FCS. At given xy coordinates on the bilayer, we have measured the autocorrelation functions at different axial z distances and fitted each autocorrelation function using equation 2 to get characteristic diffusion times of lipids. The obtained diffusion times at different z-interval for the DEC221 bilayer in the absence (Figure S2J, scatter black square points) and presence of 5 mM serotonin (Figure S2K, scatter black square points) are fitted by equation 5 to obtain the diffusion coefficient value of lipids in the DEC221 bilayer in the absence (Figure S2J, red curve) and presence of serotonin (Figure S2K, red curve). The average diffusion coefficients of DEC221 bilayer in the absence (Figure S2L, black bar) and the presence (Figure S2L, red bar) of serotonin are (5.4 ± 0.5) and (1.6 ± 0.1) $\mu m^2 s^{-1}$. The D_T of the DEC221 bilayer decreases by (70 ± 11) %, suggesting that the DEC221 bilayer becomes more ordered in the presence of serotonin.

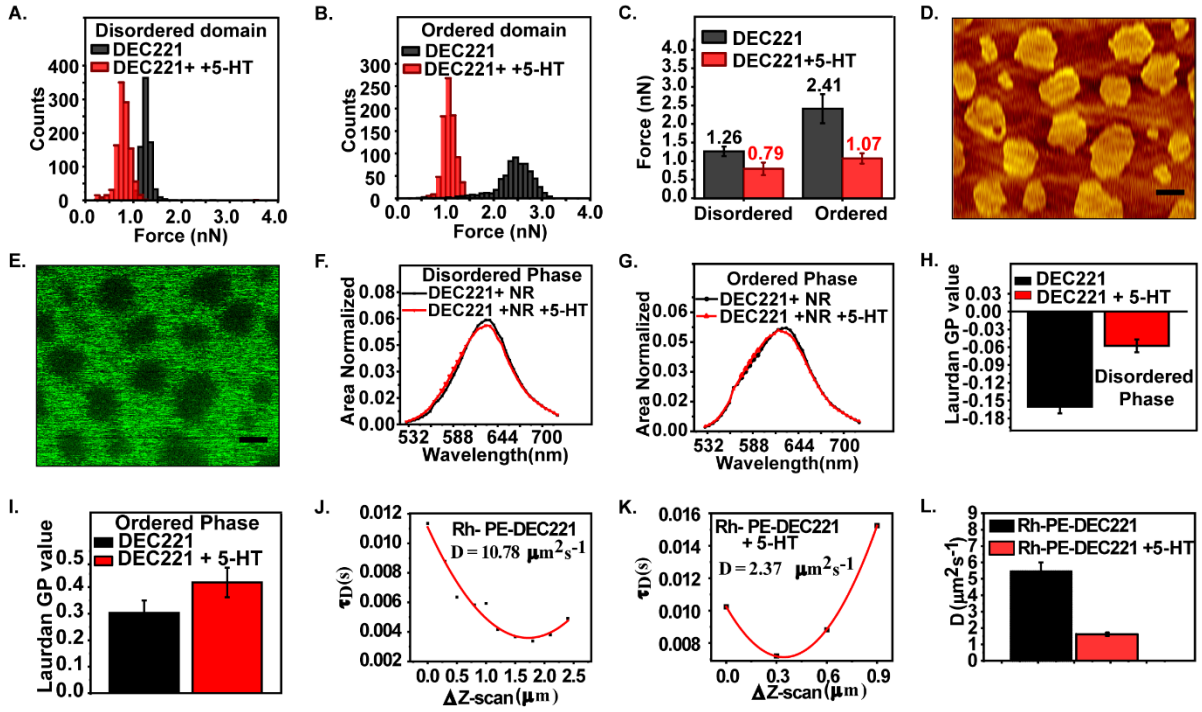

Figure S2. Effect of serotonin on the membrane properties of biphasic DEC221 bilayer. (A and B) The representative histograms of BFs on the disordered and ordered phases of DEC221 bilayer in the absence (black) and presence (red) of 5 mM serotonin (reproduced from Dey et al.[25]). (C) Average F_X of DEC221 bilayer in the disordered and ordered phases in the absence (black) and presence (red) of serotonin (reproduced from Dey et al.[25]). The numbers shown on each bar are the average F_X value. (D and E) A representative AFM and confocal images of DEC221 SLB incubated with ~ 100 nM Nile Red. Scale bar = 1μm. (F-G) The fluorescence spectra of membrane-bound Nile Red dye in the disordered (F) and ordered (G) phases of DEC221 bilayer in the absence (black) and presence (red) of 5mM serotonin (average of N = 3 measurements). (H-I) GP value of Laurdan dye in the disordered (H) and ordered (I) phases of DEC2211 bilayer in the absence (black) and presence (red) of 5mM

serotonin (average of N = 4 measurements). (J-K) Probing diffusion coefficient of DEC221 bilayer containing 0.5 mol% Liss Rhod PE by z-FCS. Representative scatter plots of diffusion times of Liss Rhod PE in the DEC221 bilayer in the absence (J) and presence (K) of 5mM serotonin at different z intervals (black square points) and fitted by equation 5 (red curve) to obtain the diffusion coefficient of DEC221 bilayer. (L) D_T of DEC221 bilayer in the absence (black) and presence (red) of 5mM serotonin (average of N = 2 measurements). Error bar is S.E.M. All experiments are carried out in the water.

References:

(1) Leonenko, Z. V.; Carnini, A.; Cramb, D. T. Supported Planar Bilayer Formation by Vesicle Fusion: The Interaction of Phospholipid Vesicles with Surfaces and the Effect of Gramicidin on Bilayer Properties Using Atomic Force Microscopy. *Biochim. Biophys. Acta - Biomembr.* **2000**, *1509* (1–2), 131–147. https://doi.org/10.1016/S0005-2736(00)00288-1.

(2) Hutter, J. L.; Bechhoefer, J. Calibration of Atomic-force Microscope Tips. *Rev. Sci. Instrum.* **1998**, *64* (7), 1868. https://doi.org/10.1063/1.1143970.

(3) Gupta, A.; Dey, S.; Bhowmik, D.; Maiti, S. Coexisting Ordered and Disordered Membrane Phases Have Distinct Modes of Interaction with Disease-Associated Oligomers. *J. Phys. Chem. B* **2022**, *126* (5), 1016–1023. https://doi.org/10.1021/ACS.JPCB.1C09421/ASSET/IMAGES/LARGE/JP1C09421_0003.JPEG.

(4) Kumar Maity, B.; Das, A.; Dutta, S.; Maiti, S. Design and Construction of a Line-Confocal Raman Microscope for Sensitive Molecules. https://doi.org/10.1007/s40010-018-0517-3.

(5) Davis, J. H.; Jeffrey, K. R.; Bloom, M.; Valic, M. I.; Higgs, T. P. Quadrupolar Echo Deuteron Magnetic Resonance Spectroscopy in Ordered Hydrocarbon Chains. *Chem. Phys. Lett.* **1976**, *42* (2), 390–394. https://doi.org/10.1016/0009-2614(76)80392-2.

(6) Huster, D.; Arnold, K.; Gawrisch, K. Influence of Docosahexaenoic Acid and Cholesterol on Lateral Lipid Organization in Phospholipid Mixtures. *Biochemistry* **1998**, *37* (49), 17299–17308. https://doi.org/10.1021/bi980078g.

(7) Lafleur, M.; Fine, B.; Sternin, E.; Cullis, P. R.; Bloom, M. Smoothed Orientational Order Profile of Lipid Bilayers by 2H-Nuclear Magnetic Resonance. *Biophys. J.* **1989**, *56* (5), 1037–1041. https://doi.org/10.1016/S0006-3495(89)82749-3.

(8) Dey, S.; Surendran, D.; Engberg, O.; Gupta, A.; Fanibunda, S. E.; Das, A.; Maity, B. K.; Dey, A.; Visvakarma, V.; Kallianpur, M.; Scheidt, H. A.; Walker, G.; Vaidya, V. A.; Huster, D.; Maiti, S. Altered Membrane Mechanics Provides a Receptor-Independent Pathway for Serotonin Action. *Chem. - A Eur. J.* **2021**, *27* (27), 7533–7541. https://doi.org/10.1002/chem.202100328.